

# An assessment of ground-based GNSS Zenith Total Delay observation errors and their correlations using the Met Office UKV model

G. V. Bennett,<sup>a\*</sup> H. R. Johnson,<sup>a</sup> P. P. Weston,<sup>b</sup> J. Jones<sup>a</sup> and E. Pottiaux<sup>c</sup>

<sup>a</sup>Met Office, Exeter, UK

<sup>b</sup>ECMWF, Reading, UK

<sup>c</sup>Reference Systems and Planetology, Royal Observatory of Belgium, Brussels, Belgium

\*Correspondence to: G. V. Bennett, Met Office, FitzRoy Road, Exeter EX1 3PB, UK.

E-mail: gemma.halloran@metoffice.gov.uk

This article is published with the permission of the Controller of HMSO and the Queen's Printer for Scotland.

Ground-based GNSS Zenith Total Delay (ZTD) observations have been assimilated into the Met Office numerical weather prediction (NWP) models since 2007, and into the Met Office UKV model since its introduction in 2009. The UKV model is a 1.5 km resolution convective-scale model and uses a 3D-Var assimilation system. There is a plan to upgrade the UKV assimilation system from 3D-Var to 4D-Var in the near future, giving the opportunity to increase the temporal resolution of ZTDs assimilated. The ZTD observation-error covariances used operationally are assumed to be uncorrelated in both space and time despite the expectation that ZTDs have temporally and spatially correlated observation errors due to the production method (e.g. batch processing using a sliding window and (time) relative constraints). To assess whether these error correlations should be accounted for in order to use ZTDs at higher temporal resolution, *a posteriori* diagnostics to estimate the extent of temporal and spatial error correlations in ZTD observations over the UK, BENELUX and Northern France are used.

Over two separate month-long periods, we find that ZTD observations within the same processing batch are correlated, and that correlations persist between different batches to at least 1 h. Spatially, ZTD observations are found to be correlated to a minimum of 62.5 km. We find that the extent of the diagnosed correlation between observations separated in space and time is affected by the value of the relative constraints parameter chosen by the processing centre in the GNSS processing software. The impact of the relative constraints parameter on the diagnosed error variances is greater than that revealed by innovation statistics alone.

**Key Words:** zenith total delay; GNSS; error correlation; NWP; UKV

Received 2 March 2017; Revised 6 June 2017; Accepted 12 June 2017; Published online in Wiley Online Library 23 August 2017

## 1. Introduction

The potential of using signals from Global Navigation Satellite System (GNSS) satellites for meteorology was recognised by Bevis *et al.* (1992) over 20 years ago. The equivalent extra path travelled by a GNSS satellite signal when passing from the satellite to a ground-based receiver through the neutral atmosphere is expressed as the total path delay in the zenith direction above the receiver, known as the Zenith Total Delay (ZTD). Each ZTD observation is comprised of slant path delays to several satellites within an observed epoch, which are mapped to the zenith direction by mapping functions, e.g. Niell Mapping Functions (NMFs; Niell, 1996), Global Mapping Functions (Boehm *et al.*, 2006a), Vienna Mapping Functions (Boehm *et al.*, 2006b).

Thanks to the Economic Interest Grouping (EIG) EUMETNET GNSS Water Vapour Programme (E-GVAP; <http://egvap.dmi.dk>;

accessed 4 July 2017), ZTD observations are available on the Global Telecommunication System (GTS) in near-real time from networks of GNSS receivers across Europe, but also world-wide. These ZTDs are produced by national geodetic, cartographic and meteorological institutes using a range of software, e.g. the Bernese GNSS Software 5.0 (Dach *et al.*, 2007) or GAMIT (Herring *et al.*, 2009). National networks of GNSS receivers are generally processed solely by their national institutes due to restrictions on the dissemination of raw GNSS data. The national processing centres also include GNSS sites from freely available networks, such as data from the European Permanent Network (EPN; <http://epncb.oma.be>, accessed 4 July 2017; Bruyninx *et al.*, 2012) or from the International GNSS Service (IGS; <http://igsceb.jpl.nasa.gov/>, accessed 4 July 2017) network to give broader coverage than their national network.

As with any observation, various sources of uncertainty are associated with ZTD measurements. In addition to the

instrumental errors introduced during the sending and receiving of GNSS signals, systematic errors can also be introduced during the processing stage. For example, mapping functions (e.g. the NMF from Niell, 1996) are used to convert several observations along slant angles to a composite observation in the zenith direction. Mapping functions have tended to assume that the atmosphere is horizontally stratified which is not always the case. This assumption will be more valid in some instances than others, and its validity is likely to vary seasonally which could lead to different levels of error correlations at different times of year. Mapping functions which use NWP model outputs to produce coefficients for mapping to the zenith have been developed (e.g. the Vienna Mapping Functions detailed in Boehm *et al.*, 2008) and may provide ZTDs which are a more accurate representation of the surrounding atmosphere.

GNSS raw observations are processed over a given observing period to produce a set of ZTD values within that period. Processing GNSS raw data requires a number of input parameters and models (e.g. for the orbit trajectories of the GNSS satellites), which may contain errors that are specific to that period. Some of these errors can impact the processing of the GNSS raw data recorded in the whole network, hence potentially introducing a systematic error to the ZTDs estimated in all stations for that period, leading to a correlation of ZTD errors within the given period.

A systematic error introduced to the GNSS processing is likely to have the effect of creating errors that are correlated with one another, either temporally or spatially. When assimilating observations for NWP, the errors associated with the observations are specified, and the covariance of errors between pairs of observations should be accounted for where possible. These errors and their covariances affect the weights given to the observation. If the weighting is too low or too high then assimilation of the observations will be suboptimal.

Within the least-squares adjustment used to calculate ZTDs, relative constraints are placed on the estimated ZTD values. Relative constraints are parameters that constrain the time evolution of the ZTDs. Wielgosz *et al.* (2011) tested four processing strategies in which they used two reference ZTD points calculated using the Saastamoinen model (Saastamoinen, 1972), and used this model to also calculate the ZTD for a small network of receivers with baselines of 1–3.2 km. They varied the relative constraints between 0.1 and 100.0 mm. Applying relative constraints of 0.1 mm resulted in ZTD differences of less than 3 mm between the network receivers during the test periods, whereas with relative constraints of 100.0 mm the ZTDs varied by as much as 42 mm. The degree to which the ZTD should vary in such cases depends on the atmospheric conditions. Rohm *et al.* (2014) studied the rate of change of ZTD for a selection of GNSS receivers in the Melbourne region in Australia during ‘normal’ and ‘storm’ conditions. During storm conditions they found that the average rate of change of ZTD was  $40 \text{ mm h}^{-1}$  compared to  $20 \text{ mm h}^{-1}$  in normal conditions. They concluded that the relative constraints during stormy conditions should be increased by a factor of 2. This would enable the measured ZTD to better represent the fluctuations in the atmosphere. During normal stable conditions, noise in the measured ZTD could be kept to a minimum.

Following a preliminary study by Higgins (2001), Bennitt and Jupp (2012) reported on the earliest assimilation trials at the Met Office, using the North Atlantic and European (NAE) numerical weather prediction (NWP) model with both 3D and 4D variational assimilation (3D-Var and 4D-Var). The NAE and UK4 model cited by Bennitt and Jupp (2012) are now obsolete, and the Met Office now focuses its assimilation resources on the global and 1.5 km horizontal resolution UK model, called the UKV. Bennitt and Jupp (2012) used an 8 mm observation error for all observations in their four trial periods when assimilating into the NAE model at both 24 and 12 km horizontal resolution. When assimilating with 4D-Var, the ZTD observations were thinned to one observation per hour in the 6 h assimilation window of

the NAE, with each observation chosen to be closest to the full hour. Using this thinning approach, little impact was found when assimilating ZTDs with 4D-Var compared to 3D-Var in the NAE. It was noted that better diagnostics for choosing the observation error and an improved thinning strategy for ZTDs could be beneficial to the Met Office. Due to a constant process of refining and improving both NWP models and assimilation processes, the considerations for assimilation of ZTDs have changed since the earlier study of Bennitt and Jupp (2012).

Macpherson *et al.* (2008) chose to apply the temporal observation error model of Jarvinen *et al.* (1999) for their ZTD assimilation experiments using the Environment Canada (EC) regional NWP model at 15 km horizontal resolution. A 6 h time window was used in the EC regional model, with a series of nine observations from each site. The temporal error correlation model used by Macpherson *et al.* (2008) was based on the findings of Stoew and Elgered (2005), who estimated the temporal error correlation of ZTDs based on the errors in the position of the GNSS receivers as calculated by the software used to produce the ZTD. Using these position errors, temporal correlations were found out to 1–2 days, which Macpherson *et al.* (2008) suggested was due to satellite orbit geometry. Acknowledging the work of Eresmaa and Jarvinen (2005), who found correlation in ZTD errors out to 100–200 km, Macpherson *et al.* (2008) chose a spatial thinning distance of 100 km. ZTDs were found to give a positive impact on precipitation forecasts in most cases when assimilating with 4D-Var in the EC NWP models.

Poli *et al.* (2007) assessed the impact of assimilating ZTDs using 4D-Var into the T358 (approximately 23 km resolution over France) resolution global Arpège NWP model. Using a 6 h assimilation window with seven time slots, Poli *et al.* (2007) assimilated the average ZTD value from the observations within each time slot. Observations were thinned to a horizontal distance of 50 km, and the observation error for each of three trials was varied from 4.5 to 10 mm according to the season, based on studying the innovation statistics. Poli *et al.* (2007) found a positive impact on forecasting the synoptic circulation when assimilating ZTDs, and a positive impact on precipitation in spring and summer. Based on these trials, Poli *et al.* (2007) attempted to diagnose the background and observation errors, using the technique of Desroziers *et al.* (2005). Taking statistics from eight assimilation cycles from each of their three trial periods, observation error estimates of between 5 and 7 mm were found. Using the method of Andersson *et al.* (2000), they diagnosed the background error for ZTD in the Arpège model to be approximately 10 mm in winter and 25 mm for summer in Europe. Consequently, Poli *et al.* (2007) chose to set ZTD observation errors of 10 and 20 mm for the winter and summer respectively in their operational assimilation, in order to preserve the ratio of the background and observation errors in each season at 1.0 for winter and 0.8 for summer.

Observation-error statistics can be estimated using *a posteriori* diagnostics such as those proposed by Desroziers *et al.* (2005) and Hollingsworth and Lönnberg (1986). Such diagnostics have previously been used to estimate the error characteristics of hyperspectral infrared sounders such as IASI and AIRS (Garand *et al.*, 2007; Stewart, 2009; Bormann *et al.*, 2010; Stewart *et al.*, 2013; Weston *et al.*, 2014), microwave sounders such as AMSU-A and MHS (Bormann and Bauer, 2010) and microwave imagers such as SSM/I and AMSR-E (Bormann *et al.*, 2011).<sup>\*</sup> The same method can be used on any type of observation which is assimilated. Here we apply the method to ZTD observations specifically.

The characteristics of observation errors which can be diagnosed include the error standard deviations as well as spatial (both vertical and horizontal), inter-channel and temporal

<sup>\*</sup>IASI = Infrared Atmospheric Sounding Instrument; AIRS = Atmospheric Infrared Sounder; AMSU-A = Advanced Microwave Sounding Unit; MHS = Microwave Humidity Sounder; SSM/I = Special Sensor Microwave/Imager; AMSR-E = Advanced Microwave Scanning Radiometer.

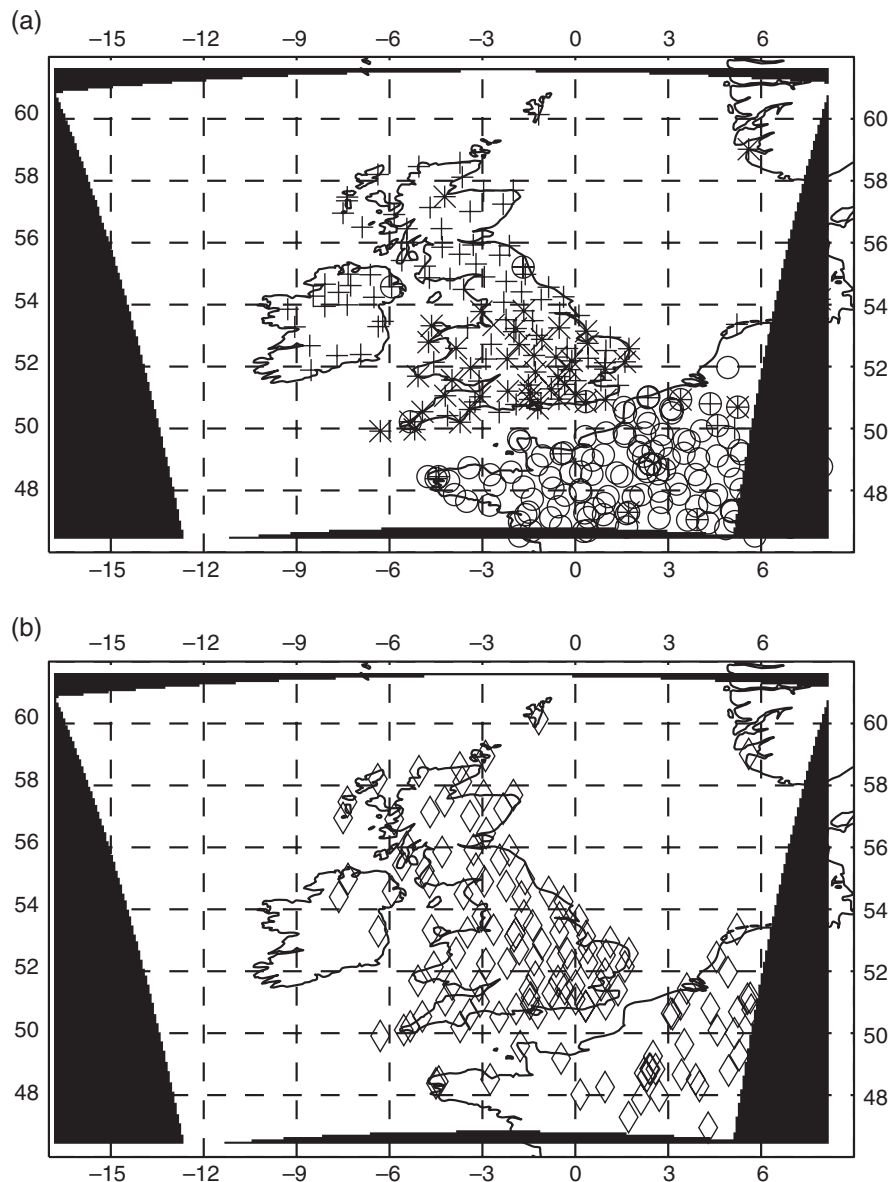


**Figure 1.** Domain of the UKV model area (white area) showing distribution of GNSS receiver sites for processing centres (a) METO (+), METR (x) and SGN (o) and (b) ROB1-4.

error correlations. For example, if observation pairs are binned by horizontal separation and observation error estimates are produced for each bin, then spatial observation error correlations can be diagnosed as explained and illustrated in Bormann and Bauer (2010). In a similar way, vertical or inter-channel error correlations can be diagnosed by binning observations by vertical level or channel number as in Bormann and Bauer (2010); Bormann *et al.* (2010, 2011); Garand *et al.* (2007); Stewart (2009); Stewart *et al.* (2013); Weston *et al.* (2014). The method can also be extended to diagnose temporal error correlations by binning observation pairs by temporal separation and calculating observation error estimates for each bin.

The Met Office plans to move from 3D-Var assimilation towards using 4D-Var assimilation for the UKV model (Tang *et al.*, 2013), so it is especially important that we understand the temporal error correlations between observations. In this article we diagnose and study the statistics of ZTD observation errors, including temporal and spatial error correlations as well as the error standard deviations within the Met Office UKV model across the whole assimilation window.

In section 2 of this paper we describe the methods used to diagnose the observation errors and their correlations. Section 3 describes the results of the experiments we have run to diagnose the ZTD error correlations, with discussion of these results and their implications in section 4. In section 5 we summarize our conclusions from these results.

## 2. Theory and methods

### 2.1. Experimental set-up

The Met Office UKV model is a variable-resolution NWP model based on the dynamics described by Davies *et al.* (2005). The UKV model domain is shown in Figure 1; it has a resolution of 1.5 km over mainland UK stretching to 4 km resolution near the edges of the domain, and in total there are  $744 \times 928$  gridpoints and 70 vertical levels with a model top at approximately 40 km. ZTD observations are assimilated operationally into this model with an analysis grid at a resolution of 3 km using 3D-Var. Other observations assimilated into this model are AMDAR reports from aircraft, radiosonde profiles, surface SYNOP, scatterometer winds, atmospheric motion vectors, clear-sky radiances from SEVIRI, Doppler radial winds, GeoCloud (Renshaw and Francis, 2011), MHS and surface-based cloud observations.<sup>†</sup>

The assimilation is run every 3 h, with an analysis at 0000, 0300, 0600, 0900, 1200, 1500, 1800 and 2100 UTC. A 3 h time window is used, centred on the analysis times listed above. In this study, we assimilate all ZTD observations within the time window. We ran the assimilation cycles for a summer and a winter period: 19 May

<sup>†</sup>AMDAR = Aircraft Meteorological Data Relay; SEVIRI = Spinning Enhanced Visible and Infrared Imager.

Table 1. Temporal separations for ZTD observations from METO, ROB and SGN relative to the first hourly batch of observations, within a 3 h assimilation window.

Obs. time (min)	HH = 1					HH = 2					HH = 3				
	0	15	30	45	59	0	15	30	45	59	0	15	30	45	59
0	0	15	30	45	59	60	75	90	105	119	120	135	150	165	179
15	15	0	15	30	44	45	60	75	90	104	105	120	135	150	164
30	30	15	0	15	29	30	45	60	75	89	90	105	120	135	144
45	45	30	15	0	14	15	30	45	60	74	75	90	105	120	134
59	59	44	29	14	0	1	16	31	46	60	61	75	90	105	119

Table 2. Temporal separations for ZTD observations from METR relative to the first 15 min batch of observations, within a 3 h assimilation window.

Obs. time (min)	0	14	15	29	30	44	45	59
HH = 1								
0	0	14	15	29	30	44	45	59
14	14	0	1	15	16	30	31	45
HH = 2								
0	60	74	75	89	90	104	105	119
14	46	60	61	75	76	90	91	105
HH = 3								
0	120	134	135	149	150	164	165	179
14	106	120	121	135	136	150	151	165

2013 to 18 June 2013 and 1 December 2013 to 31 December 2013. Model background fields were available at analysis time (T+0), and each of the 2 h either side of the analysis time (T-2, T-1, T+1, T+2). Background ZTD values at intermediate times to these fields are therefore interpolated from the nearest hourly fields.

From 19 May to 18 June 2013, the UK experienced a mixture of weather regimes, with some periods of fairly stable weather and high pressure, and some periods influenced by low pressure systems. The month of December 2013 was windier than average over the UK, with a series of low pressure systems influencing the weather, bringing heavy rain and flooding.

For each of the two monthly periods studied, we ran the assimilation system a number of times, selecting a different ZTD processing centre each time. These processing centres are METO (the Met Office hourly processed Europe-wide ZTD observations), SGN (the French National Institute of Geographic and Forest Information hourly processed ZTD observations), METR (the Met Office 15 min processed UK-wide ZTD observations) and ROB (Royal Observatory Belgium). An overview of the different methods commonly used in ZTD processing can be found in Guerova *et al.* (2016). The processing centres provide ZTD observations at locations as seen in Figure 1. These processing centres all used the Bernese GNSS Software v5.0 (Dach *et al.*, 2007) and IGS ultra-rapid orbit products. METO, ROB and SGN provide ZTD observations in hourly batches, using a double-difference processing method, and a sliding window approach for the normal equation (NEQ) files from previous hours' processing, but providing ZTD values only from the last hour for data assimilation. ROB uses 3 h of NEQs plus the current hour, METO uses 4 h worth of NEQ files plus the current hour, whereas SGN use 6 h of NEQs plus the current hour. The ZTD observations for the hour HH are provided at HH00, HH15, HH30, HH45 and HH59 min. Within the 3 h assimilation window, this gives the temporal separations as given in Table 1. METR provides observations in 15 min batches, using 16–20 15 min NEQ files from the previous 4 h. Within the hour HH, METR ZTD observations are provided at HH00, HH14, HH15, HH29, HH30, HH44, HH45 and HH59 min which gives the temporal separations as given in Table 2. ROB provided ZTD observations in four different datasets for the December 2013 period, denoted as ROB1, ROB2, ROB3, and ROB4, which used relative constraints of 1.0, 2.0, 4.0, and 7.0 mm respectively. SGN, METO and METR all use relative constraints of 1.0 mm.

## 2.2. ZTD observation pre-processing

ZTD observations were passed through the standard quality control procedures which are used for operational assimilation. Firstly, GNSS sites where the difference in height between the surface and the model surface is greater than 300 m are rejected. When the observation site lies too far above or below the model surface, the observation operator does not give a good representation of the humidity near the surface, which can lead to problems in the assimilation process. Secondly, in order to avoid assimilating spurious observations, ZTDs are rejected when the absolute innovation (observation minus background) value is greater than 55 mm (five times the maximum standard deviation found in long-term monitoring of the innovations (Bennett and Jupp, 2012)).

A bias correction is applied to the ZTD observations based on their specific processing centre and site identification code. Bias correction values are computed from the mean innovation over 28 days, which should be sufficient to account for any bias in measurement or forward model error, but not be heavily influenced by synoptic model bias (Bennett and Jupp, 2012). The bias correction values are updated when significant changes in the model occur, or to take into account seasonal or long-term drift. If the available bias correction value is calculated from less than 7 days of innovation data, the observations from the site are rejected. In that case, the data sample is not considered sufficient to capture the true bias.

For these experiments, no temporal or spatial thinning of ZTD observations was applied, as we wished to capture the innovations and residuals from all ZTD observations from the chosen GNSS site and chosen processing centre. ZTD observations comprised approximately 3% of the total observations assimilated in each cycle. In each experiment, observations from only one processing centre were chosen. The observations are assigned an observation error of 6 mm, which is the value currently used for operational assimilation in the UKV model. This observation error value was prescribed following previous testing of different error values between 3 and 12 mm.

## 2.3. Data assimilation

An NWP model requires initial conditions as a starting point for any forecast run. As the current state of the atmosphere is unknown, a best estimate of this true state is produced using data assimilation. Millions of observations are combined with a previous short-range model forecast (known as the background) to produce an analysis at model resolution. This process is performed by minimizing a cost function of the form

$$J(\mathbf{x}) = \frac{1}{2} (\mathbf{x} - \mathbf{x}^b)^T \mathbf{B}^{-1} (\mathbf{x} - \mathbf{x}^b) + \frac{1}{2} \sum_{i=1}^n \{y_i - H_i M_i(\mathbf{x})\}^T \mathbf{R}_i^{-1} \{y_i - H_i M_i(\mathbf{x})\}, \quad (1)$$

where  $\mathbf{x}$  is the model state vector,  $\mathbf{x}^b$  is the background state vector produced from a previous short-range forecast,  $y_i$  is the vector of observations valid at time  $i$ ,  $\mathbf{B}$  is the background-error

Table 3. Diagnosed observation-error standard deviations (mm) for the summer and winter periods, and the mean (standard deviation) innovation for the period, for each processing centre.

	19 May–18 June 2013		December 2013	
	Diagnosed obs error $\sigma$	Mean ( $\sigma$ ) innovations	Diagnosed obs error $\sigma$	Mean ( $\sigma$ ) innovations
METO	5.29	0.95 (8.62)	6.09	-0.78 ( 9.18)
METR	5.30	4.58 (8.78)	6.41	-1.95 ( 9.96)
SGN	5.45	1.16 (8.74)	5.57	-2.38 ( 9.39)
ROB1	–	–	6.08	2.09 (10.47)
ROB2	–	–	7.16	2.05 (10.39)
ROB3	–	–	7.57	2.19 (10.47)
ROB4	–	–	8.08	2.29 (10.81)

covariance matrix,  $\mathbf{R}_i$  is the observation-error covariance matrix valid at time  $i$ ,  $H_i$  is the observation operator valid at time  $i$  and  $M_i$  is the forecast model which propagates the model state from time 0 to  $i$ . The observation- and background-error covariance matrices provide information on how much weight should be given to each source of information.

The diagonal elements of the  $\mathbf{R}$  matrix in Eq. (1) contain error variances for each observation and the off-diagonal elements contain the error covariances between every pair of observations. To simplify the processing, current data assimilation schemes assume that observation errors from different observation types are uncorrelated with one another, which means that this matrix is assumed to be block diagonal, with each block corresponding to a different observation type.

In the Met Office data assimilation system, inter-channel error correlations in IASI, AIRS and Cross-track Infrared Sounder (CrIS) observations are accounted for as detailed by Weston *et al.* (2014). The errors for all other observation types are assumed to be uncorrelated so that each block of the main  $\mathbf{R}$  matrix is diagonal and all off-diagonal elements are set to zero. This means that all other forms of error correlation, including spatial and temporal correlations, are assumed to be zero.

Spatial and temporal error correlations are known to exist in some observation types such as atmospheric motion vectors, which are wind observations derived by feature tracking in satellite images (Bormann *et al.*, 2003). However, rather than being accounted for directly, the data are thinned so that no two observations with a spatial or temporal separation of less than 200 km or 2 h can be assimilated, and the observation errors are inflated.

#### 2.4. Estimation of observation errors

To estimate the observation-error standard deviations and temporal and spatial correlations, the diagnostic procedure introduced by Desroziers *et al.* (2005) is used here. In addition to this method, there are other methods of estimating observation errors such as that proposed by Hollingsworth and Lönnberg (1986), which Eresmaa and Jarvinen (2005) adapted in their study for estimating the spatial error covariance of ZTDs. Eresmaa and Jarvinen (2005) used a combination of the errors at analysis time of Integrated Water Vapour from radiosondes, surface pressure from SYNOP stations, and the ZTD from GNSS to compute a spatial error covariance model for ZTDs using Hollingsworth and Lönnberg (1986)'s method. However, this method attempts to split an estimate which contains contributions from both the background and observation errors by assuming that, whilst the background errors are spatially correlated, the observation errors are not. Our study aims to diagnose both temporal and spatial observation error correlations, therefore violating the spatial correlation assumption, hence Hollingsworth and Lönnberg (1986)'s method is not applicable. For this reason the diagnostic method proposed by Desroziers *et al.* (2005) is the only method used to estimate observation errors in this article.

The chosen method uses observation minus background (innovation) and observation minus analysis (residual) statistics to produce observation-error variances and covariances. The basic formula for calculating these diagnostics is

$$\mathbf{R} = \mathbf{E} \left[ \left\{ \mathbf{y} - H(\mathbf{x}^a) \right\} \left\{ \mathbf{y} - H(\mathbf{x}^b) \right\}^T \right], \quad (2)$$

where the notation is as in section 2.3,  $\mathbf{E}$  is the expectation, and the analysis,  $\mathbf{x}^a$ , is defined as the model state for which the cost function value in Eq. (1) is minimized.

There are two key assumptions made in the derivation of Eq. (2). The first is a standard data assimilation assumption that the observation and background errors are uncorrelated. The second assumption is that the assumed  $\mathbf{R}$  and  $\mathbf{B}$  matrices used to produce the analysis are consistent with the true error covariance matrices. If either of these assumptions are violated then the diagnostic can produce some unrealistic results such as correlation values of greater than 1.0. Additionally it has been shown by Desroziers *et al.* (2009) that, to obtain accurate estimates from this diagnostic, the observations and background errors must have significantly different scales.

In our case, we are attempting to diagnose non-zero temporal and spatial observation error correlations which are assumed to be zero within the assimilation scheme. This is a direct violation of the second assumption above. This means that any results from this diagnostic should be interpreted with caution. The length-scales of the humidity background errors in the UKV model vary from  $\sim 5$  to 30 km, whereas the length-scales of the ZTD observation errors have been found to be significantly longer at 100–200 km in the previous study by Eresmaa and Jarvinen (2005). This means that a lack of scale separation should not have an impact on the results.

To estimate the observation-error standard deviations, the square root of Eq. (2) is used with the innovation and residual values coming from the same observations as shown by

$$\sigma = \sqrt{\frac{1}{n} \sum_{i=1}^n \left\{ y_i - H^i(\mathbf{x}^a) \right\} \left\{ y_i - H^i(\mathbf{x}^b) \right\}}, \quad (3)$$

where  $H^i$  is the observation operator which takes the model state to the observation equivalent at the same location and time as  $y_i$ , and  $n$  is the number of observations in the sample.

To estimate the error covariances, Eq. (2) is used with innovation and residual values coming from different observations with a certain temporal or spatial separation as shown by

$$cov = \frac{1}{\sum_{i=1}^n m_i} \sum_{i=1}^n \sum_{j=1}^{m_i} \left\{ y_i - H^i(\mathbf{x}^a) \right\} \left\{ y_j - H^j(\mathbf{x}^b) \right\}, \quad (4)$$

where  $m_i$  is the number of observations which are at a certain spatial or temporal separation from  $y_i$ . This formula is then used for many different bins of separation distances and times to

calculate the error covariances for all separations. To calculate the non-dimensional correlation value, the covariances are divided by the variance (or covariance at zero separation).

In each case, for both temporal and spatial error correlations, we wish to isolate one type of correlation from the other. When calculating temporal error correlations, only observation pairs at the same location are used to remove the effect of spatial error correlations on the data. When calculating spatial error correlations, only observation pairs which have a maximum temporal separation of 15 min are used. This is a compromise between choosing the smallest time separation to avoid unwanted effects from temporal correlations whilst maintaining a large enough sample size for each separation bin to give statistically significant results. For larger temporal separation thresholds, the diagnosed spatial correlations will be dampened by the effect of weaker temporal correlations at larger separations. Conversely, using larger temporal separations may introduce spurious correlations due to water vapour features advecting between different sites and the same feature being detected in two different sites at two different times.

In order to convey the statistical significance of the correlations, we calculated the 95% confidence intervals. The confidence intervals are calculated by taking the standard deviation of the diagnosed correlation values and dividing by the square root of the sample size for the corresponding separation bin. In statistics it is generally agreed that correlation values of below 0.2 are negligible.

### 3. Results of diagnostics

#### 3.1. Innovation analysis

The mean innovations for December 2013 vary from  $-2.38$  mm (SGN) to  $2.29$  mm (ROB4) with an average standard deviation across the seven observation datasets of  $10.10$  mm (Table 3 and Figure 2). The mean innovations for the May–June period have a larger range than the December period ( $0.95$ – $4.58$  mm) with an average standard deviation of  $8.71$  mm (Table 3 and Figure 2). Figure 2 shows that the different mean innovations for each processing centre correspond to systematic shifts in the distribution of innovations. The mean innovations for ROB increase slightly as the value of the relative constraints increase (i.e. the strength of the time constraints decrease), with ROB1 having the lowest mean innovations of  $2.09$  mm, and ROB4 having the highest of  $2.29$  mm. There is also a corresponding increase in standard deviation from  $10.47$  mm (ROB1) to  $10.81$  mm (ROB4).

The diagnosed observation error standard deviations for METO, METR and SGN for December 2013 are  $6.09$ ,  $6.41$ , and  $5.57$  mm respectively (Table 3). For the May–June period, the diagnosed observation-error standard deviations have a smaller range than in the December 2013 period, ranging from  $5.29$  mm (METO) to  $5.45$  mm (SGN) (Table 3). For ROB, the diagnosed observation-error standard deviations increase from  $6.08$  to  $8.08$  mm with increasing relative constraints.

#### 3.2. Temporal correlations

During the May–June period, METO and SGN observation errors are correlated up to 60 min for all time intervals. All observations within the same batch (14, 15, 29, 44, and 59 min) have correlated errors with decreasing correlations with time (Figures 3 and 4). For observations from METR, those within the same processing batch (14 min time interval) have the most correlated errors (Figure 5). METR observation errors had no significant correlation after 61 min in this period.

In the December period, the observation errors from METO exhibit similar behaviour to the May–June period (Figures 6 and 3). ZTD observations from SGN have significant correlation in their errors at time intervals out to more than 180 min in the December period and only a minority of time intervals have

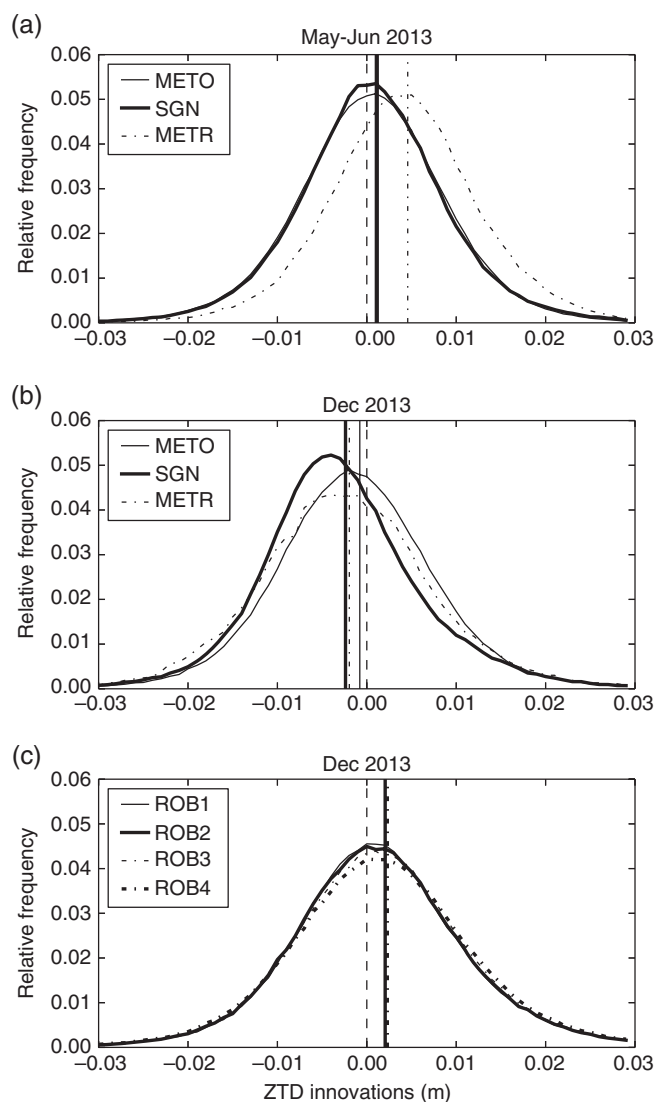


**Figure 2.** Relative frequency of ZTD innovations (observation minus background) for processing centres METO, SGN, ROB, and METR for (a) 19 May–18 June 2013 and (b, c) 1–31 December 2013. The dashed line shows zero innovation, and the vertical lines indicate the mean values.

insignificant correlations (Figure 7). Adjacent hourly batches (intervals of 1, 16, 31, 46, and 60 min) from SGN have higher error correlation values than adjacent observation batches from METO (Figures 7 and 6). Observations from METR show significant correlation until 76 min (Figure 8) compared to 61 min in the May–June period, but the 14 min correlation remains the highest in both periods (disregarding 0 min correlations). In Figures 3, 4, 6, 7, 9 and 10, the error correlation value for 14 min separations is greater than 1.0, which is not a valid value for correlation.

ZTD's from ROB1 are correlated until at least 180 min (Figure 9). ZTD observations from the same batch decorrelate faster than those from different batches. As the value of the relative constraints parameter is increased (i.e. the time evolution constraints are relaxed), from  $1.0$  mm for ROB1, to  $7.0$  mm for ROB4, the ZTD observations become decorrelated more quickly (Figures 9–12), such that for ROB4 the observations are decorrelated by 59 min. The correlation of ZTDs within the same batch decreases by a smaller amount as the value of the relative constraints increases.

#### 3.3. Spatial correlations

Spatial observation-error correlations were calculated for separation distances at  $12.5$  km intervals. Correlation is found to drop below 0.2 at separation distances of a minimum of  $62.5$  km (SGN, May–June 2013, Figure 13(a) and Table 4). The longest

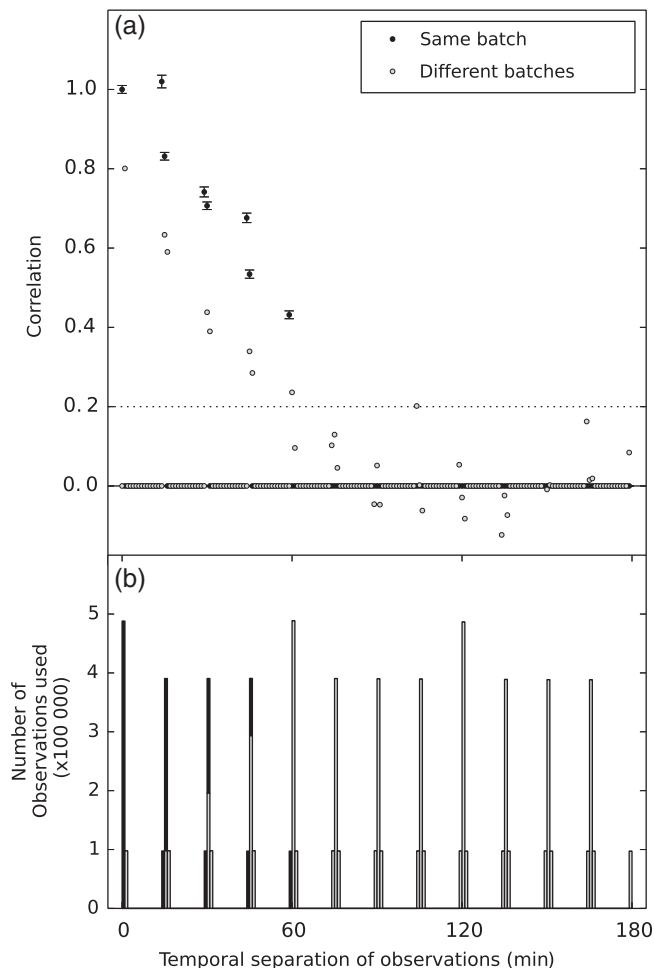


**Figure 3.** (a) Mean correlation of observations with time for ZTD observations processed by METO for 19 May–18 June 2013 at 1 min intervals, with 95% confidence intervals, and (b) the number of observation pairs used in the calculation.

separation distance after which error correlation is found to drop off in Figure 13 is 275 km (ROB1, December 2013, Table 4). Spatial correlations in December 2013 persist for greater separation distances for METO, METR, and SGN than for May–June 2013 (Figure 13(a) and Table 4).

The effect on spatial correlation of increasing the relative constraints can be seen in Figure 13(b). The spatial correlation reduces quickly up to 37.5 km for all values of relative constraints. For both ROB3 and ROB4 (relative constraints of 4.0 and 7.0 mm respectively) the correlation drops below 0.2 at 125 km separation distance. For ROB1 and ROB2 (relative constraints of 1.0 and 2.0 mm), the spatial correlation is still evident until separation distances of 275 and 250 km respectively (Figure 13(b) and Table 4).

#### 4. Discussion

Innovation statistics are often used at NWP centres when assigning a suitable observation error for use in assimilation, and we consider the standard deviation of the innovations as an indicator of the observation-error standard deviation. In the studies presented here, the innovation standard deviation values would suggest that a ZTD observation error of 8–10 mm would be suitable for use in the UKV model. Here we diagnose the average value of the observation-error standard deviation across both periods studied for METO, SGN and METR to be 5.69 mm. This suggests that the value of 6 mm currently used in the UKV model is suitable for both periods. The innovation statistics for those two periods suggest that the current rejection limit of 55 mm is too high for the UKV model. To reject observations which have innovations outside of the expected normal distribution, then a

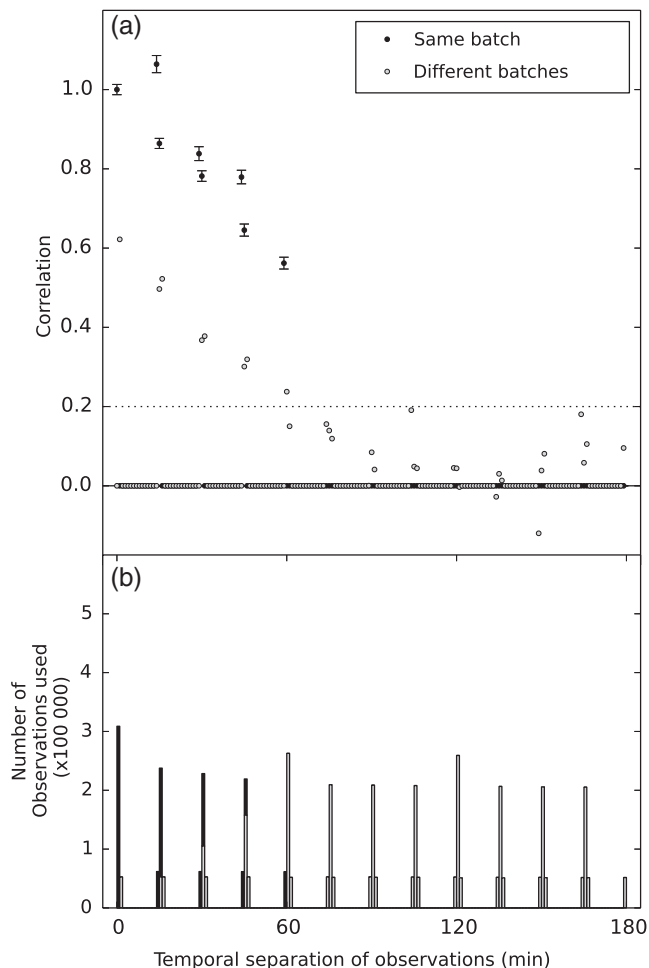


**Figure 4.** As Figure 3, but from processing by SGN.

rejection limit of five times the innovation standard deviation should be set at a minimum of 40 mm.

The innovation statistics for the ROB observations by themselves indicate that, as the relative constraints increase, there is not a clear mandate to increase the observation error for assimilation. However, using this technique we have shown that the diagnosed observation error increases by up to 2 mm as the relative constraints are increased from 1.0 to 7.0 mm. We therefore caution that innovation statistics alone may not be enough to truly advise on what the assigned observation error should be. Whilst the inflation of observation-error values such as that described by Poli *et al.* (2007) may be sufficient, it may benefit the assimilation system to consider error correlations more carefully when inflating the assigned error.

The mean innovations vary between the two seasons studied, and are also specific to a processing centre and their processing strategy. The difference in the mean innovations between seasons may be explained by the difference in model background bias between the two periods. However, we see in December 2013 that, even when processing comparable networks of receivers, the mean innovations can be quite different. The exact source of these differences is difficult to track down, due to the number of possible differences in processing strategy and is not within the scope of this study. However it is an important consideration when designing a bias-correction strategy in an assimilation system. Separating the observation bias arising from the processing strategy from the shifting nature of any model background bias is a focus of ongoing work at the Met Office, to inform the best strategy for bias correcting ZTD observations.

The difference in temporal error correlations between the two periods studied may be due to differences in the humidity characteristics of the periods. December 2013 was dominated by synoptic-scale weather patterns, which may be more likely to persist over an area for a longer period of time. During May–June

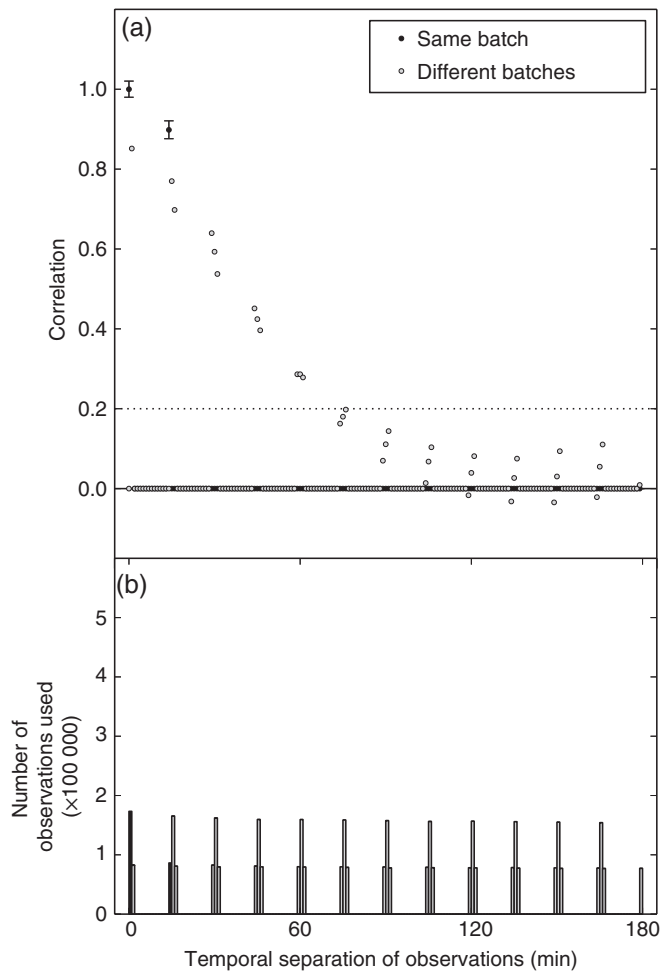


Figure 5. As Figure 3, but from processing by METR.

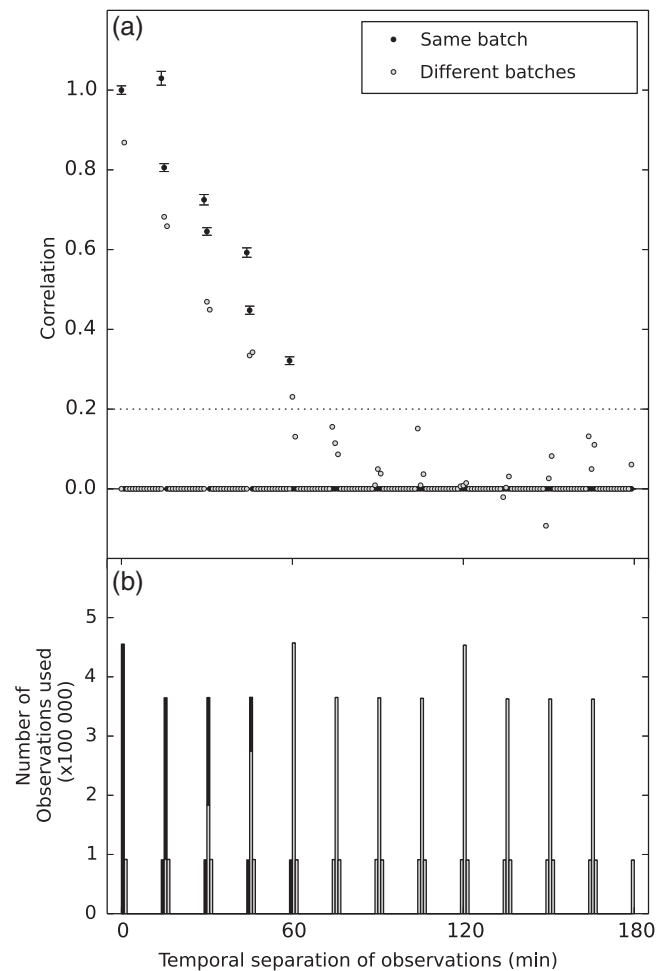


Figure 6. As Figure 3, but for 1–31 December 2013.

2013, the weather was much more varied, and so ZTD fluctuations at a site may vary more rapidly. Depending on the ability of the model to represent these temporal fluctuations, it may be less likely in the May–June case that the innovations and residuals are correlated due to rapidly evolving humidity features. The slightly greater spatial error correlation found in December 2013 also supports this, and is in agreement with the work of Rohm *et al.* (2014). The different geographical area covered by SGN compared to the other processing centres, or the longer sliding window used in the ZTD processing, may have contributed to higher temporal error correlations in December 2013.

The temporal error correlations found here suggest that if the UKV model were to be upgraded to a 4D-Var assimilation system using the same time window and background field frequency as at present (currently T–120, T–60, T+0, T+60, T+120 min), then for METO we could assimilate observations at hourly frequencies without the need to allow for temporal error correlations. For a different temporal frequency of background fields, a reanalysis of the correlations would be useful.

Figures 3–8 show that for METO, METR and SGN, there is more correlation between observations within the same processing batch than between those in different batches. Whilst this is likely to be due to the nature of the way the ZTD observations are processed, it is possible that this is an artefact of the linear interpolation of hourly model values to times within the hour. Since correlations for METR, which processes in 15 min batches, persist to at least 61 min, this seems plausible. This higher correlation should be borne in mind when assimilating ZTD observations at a temporal frequency higher than 1 h. It would also be interesting to investigate this with higher-frequency model fields where model ZTD values will be more independent. In the case of ROB, we can see that increasing the relative constraints has a greater effect on observations in different batches. For

ROB1, which uses the same relative constraints as METO, METR and SGN, ZTDs in the same batch decorrelate more quickly, yet overall, observations in different batches are more highly correlated. This suggests there are further parameters involved in the processing which affect the correlation.

In Figures 3, 4, 6, 7, 9 and 10 the diagnosed error correlation value for the 14 min time separation goes above 1.0. A correlation above 1.0 is impossible and there are a number of factors contributing to such values being diagnosed here. Firstly, and most importantly, the diagnostic procedure used makes several assumptions which have to be true to obtain accurate results, as introduced in section 2.4. One such assumption is that the assumed observation- and background-error covariance matrices used in the assimilation system must be equal to the true error covariance matrices. As we do not know what the true matrices are, and consequently the assumed matrices are estimated using a range of techniques, this assumption is almost certainly violated to some extent in the Met Office UKV assimilation system. Secondly, the correlation values are calculated by dividing the covariance values by the variance (or covariance at zero separation) and there will be uncertainty in both of these estimates, so that the uncertainty in the correlation value will be compounded.

When using a diagnostic technique such as the one chosen here, the results must be interpreted with a level of caution due to these uncertainties, but they do give some useful insight into error values and correlations. By comparing such results with those from alternative diagnostic techniques, the reliability of the diagnosed values can be assessed qualitatively, as was done by Bormann and Bauer (2010) and Bormann *et al.* (2010, 2011). This will be the subject of a future study.

The drop-off in spatial error correlations which occurs between 62.5 and 105 km in Figure 13(a) might be explained by the spatial scale of a ZTD observation. One ZTD observation is produced

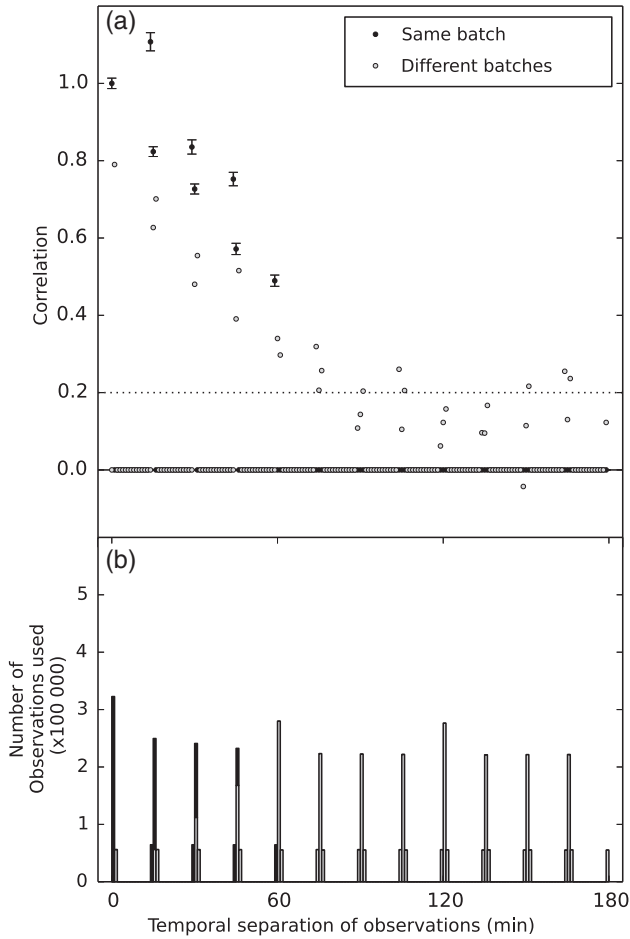


Figure 7. As Figure 4, but for 1–31 December 2013.

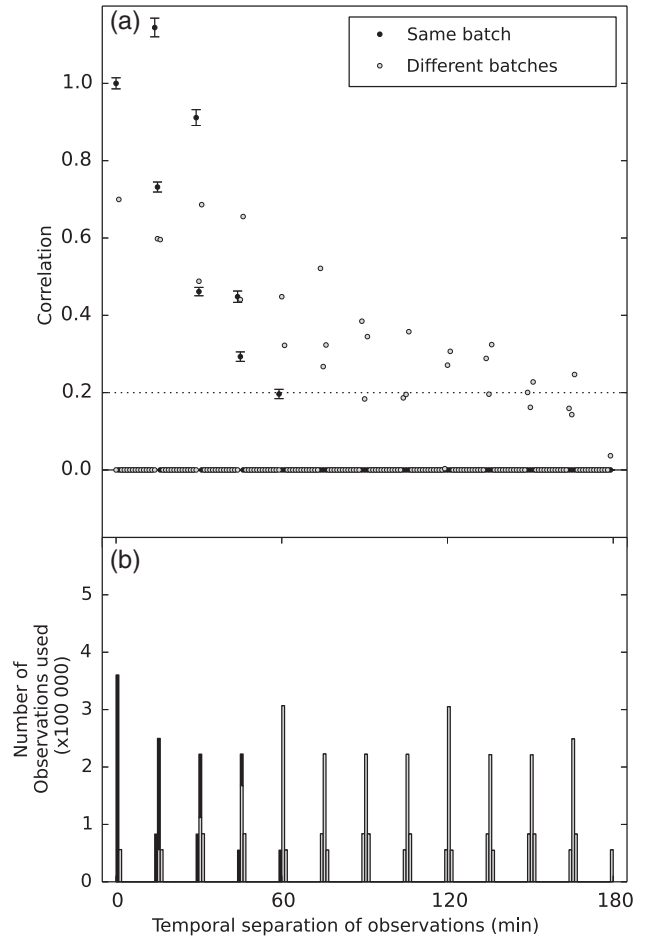


Figure 9. As Figure 3, but from processing by ROB1 for 1–31 December 2013.

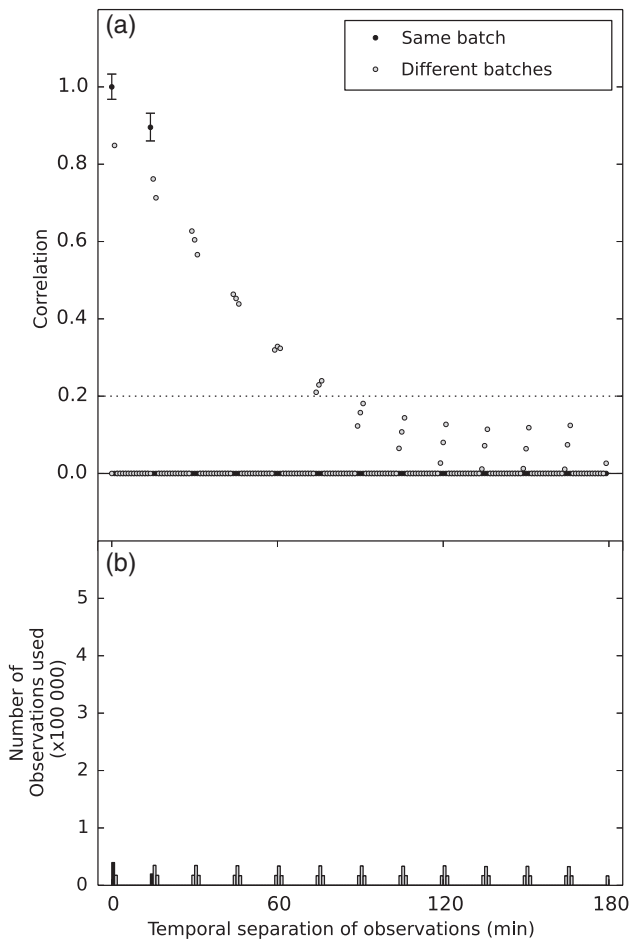


Figure 8. As Figure 5, but for 1–31 December 2013.

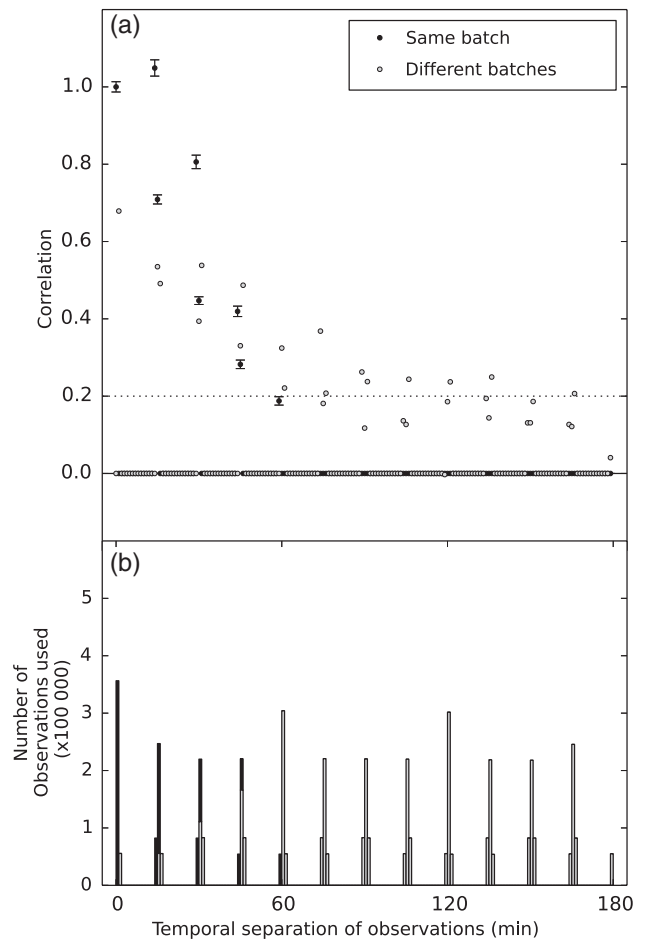


Figure 10. As Figure 9, but from processing by ROB2.

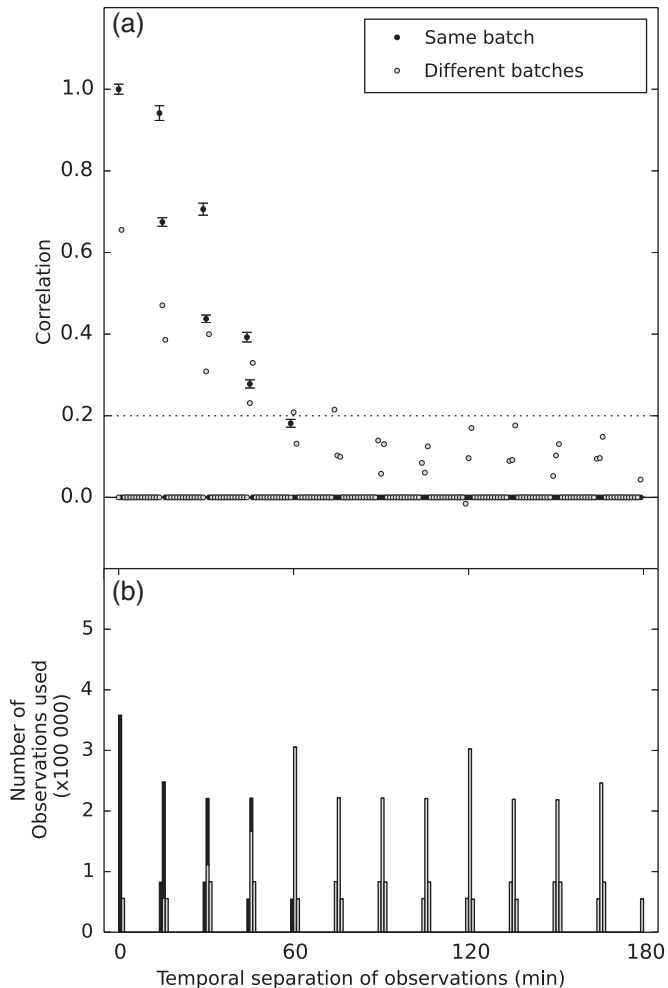


Figure 11. As Figure 9, but from processing by ROB3.

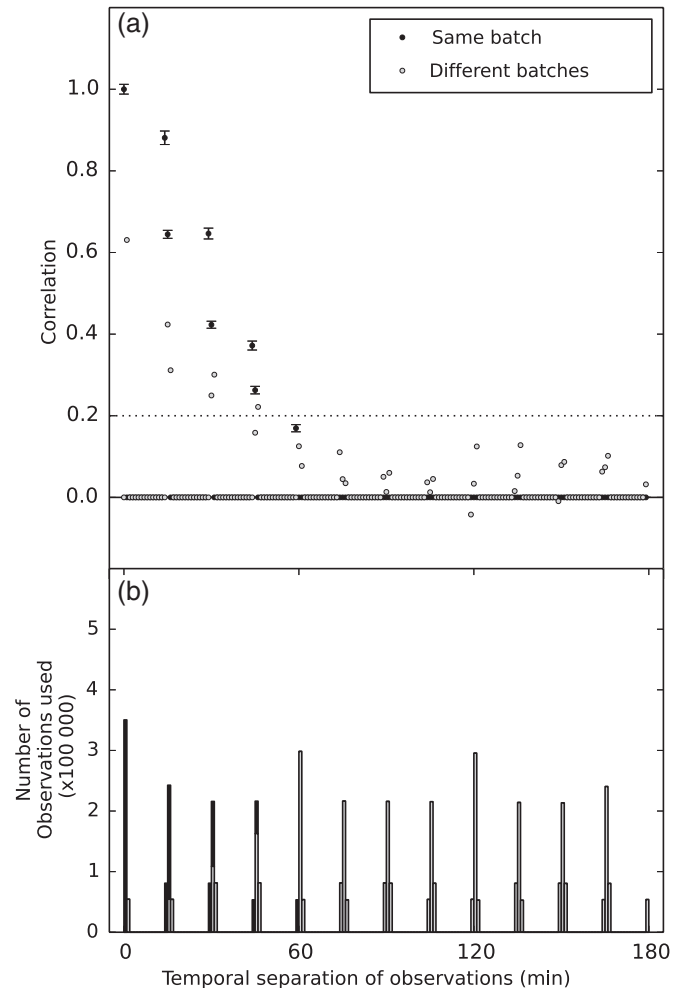


Figure 12. As Figure 9, but from processing by ROB4.

using the signal path delay from many GNSS satellites to the receiver within a given observation epoch. These signal path delays are converted to a ZTD using a mapping function. The ZTD processing system will exclude signals received from satellites at less than  $10^\circ$  elevation, due to multipath effects occurring below this angle. Therefore, we consider a ZTD observation as an observation of a cone of atmosphere above the receiver. The dominant variant in the ZTD is the delay due to water vapour in the troposphere. Since the majority of water vapour resides in the lower half of the troposphere, if we consider the top of this cone to be at 5 km altitude, the radius of the observed cone of atmosphere is approximately 55 km. The actual observed radius varies depending on the satellite constellation geometry visible from each receiver during an observation epoch. It therefore seems plausible that this cone of observation reflects in the spatial correlation of the observed ZTD value: at the lowest separation distances, the cones from adjacent receivers overlap, giving rise to correlation in the ZTDs from each site, which is captured by the innovations and residuals. This effect is likely to differ depending on the meteorological conditions. During more stable conditions, the observed atmosphere is more likely to be consistent with the atmosphere represented in the mapping function. By using more realistic meteorological information in the mapping functions, this correlation effect may be reduced, but relying on *a priori* meteorological information in order to produce an observation to be used in an assimilation system brings its own issues.

While the ZTD represents a whole-column measurement, it can be considered as having two parts: the hydrostatic delay, and the wet delay. The hydrostatic delay is closely related to the surface pressure field, and so when studying error correlations on a limited area, where pressure may be quite uniform, we could expect that there is some error correlation arising from the hydrostatic delay. By studying a global set of observations,

this effect may not be present. To isolate these effects, one could separate the hydrostatic delay and wet delay from the ZTD and study the error correlations of both.

Whilst the geometry of the ZTD observing system could explain the spatial correlation drop-off, it is clear that the processing parameters also have an effect. The influence of the relative constraints in the ROB observations on the spatial correlation is evident. By constraining the ZTD processing less, as in ROB3 and ROB4, we may be converging on what may be the true spatial correlation due to the observing geometry. ROB1 and ROB2 appear to be constrained by some other parameters which are restricting the variability as compared to METO, METR and SGN. Due to the resource constraints of the ZTD processing centres, a thorough study to pinpoint the sources of these additional correlations has not been possible, but is recommended if possible in the future. As we move towards increasingly higher-resolution NWP models, with higher variability, the ability of the ZTD observations to represent atmospheric variability becomes increasingly important. Allowing the ZTDs to capture this variability at the expense of some increase in noise, but reduction in correlation, could be beneficial.

There are relatively few GNSS receivers which are located at less than 100 km separation in the networks studied here (Figure 1). The spatial correlation scales found in this study, which are slightly shorter than the lowest correlation lengths found by Eresmaa and Jarvinen (2005), could be accounted for by applying spatial thinning to 100 km across the domain. Denser networks of GNSS receivers exist in other parts of Europe, for example in Belgium and the Netherlands, and so spatial error correlations would need to be diagnosed and accounted for if ZTDs were assimilated from these networks. Diagnosis of these spatial error correlations using a similar method and the Met Office global NWP model is planned in the near future.

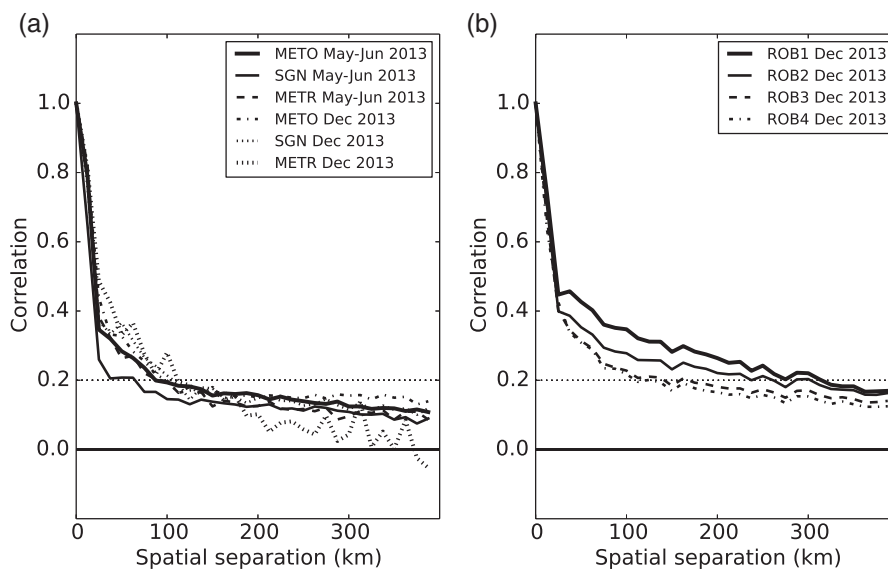


**Figure 13.** Spatial correlation of ZTD observations for 19 May–18 June 2013 and 1–31 December 2013 at 12.5 km spatial separation intervals as processed by (a) METO, METR and SGN and (b) ROB1–4.

**Table 4.** Maximum distance (km) for which significant ( $> 0.2$ ) spatial correlation has been found for ZTDs for the four processing centres METO, METR, SGN and ROB.

	19 May–18 June 2013	December 2013
METO	75	100
METR	87.5	112.5
SGN	62.5	100
ROB1	–	275
ROB2	–	250
ROB3	–	125
ROB4	–	125

At spatial scales greater than these distances, there is no significant correlation (i.e.  $< 0.2$ ).

## 5. Conclusions

Based on the diagnostics produced in this study, we have found spatial error correlations for ZTD observations with separations up to 100 km for METO and SGN processing centres, and up to 275 km for the ROB processing centre. This correlation length is consistent with the premise that a ZTD observation is produced from observations of the slant path delay of the signal from a GNSS satellite to a ground-based receiver over a given epoch, and that the geometry of these slant paths represent a cone of sky above the receiver with varying radius. Correlation exists at greater length-scales, depending on the processing settings used when producing the ZTD observations.

We have found temporal correlations in the errors of ZTD observations from the same location in the UKV model which persist to at least 1 h. The batch processing method of ZTD observations, the use of the double-difference method, NEQ stacking and which processing settings are used are likely to account for some of this correlation. The temporal frequency of model background fields also appears to be a contributing factor. Observations from within the same batch should not be assimilated in a 4D-Var assimilation without accounting for the error correlations. We find that the 6 mm observation error currently used for assimilation of ZTD observations in the UKV model using 3D-Var is appropriate. We recommend not relying on innovation statistics alone to help assign observation errors, and when considering the optimum spatial and temporal thinning of ZTD observations.

Due to the influence of model grid spacing on a model's ability to represent temporal and spatial meteorological features, we plan to run similar diagnostic experiments for ZTDs assimilated in the

Met Office global NWP model. Since the Met Office global model runs operationally at 17 km horizontal resolution and has a 6 h assimilation window with background fields every 3 h, we expect quite different results from those presented here. Ideally, we would like to see further study on the effect of the ZTD processing on the error correlations, in order to find the optimum balance of noise, correlation, and representivity in the ZTD observations. A comparison of the double difference approach and precise point positioning would also be useful to determine the effect on the spatial and temporal correlations. Such studies would help to optimize the use of ZTD in high-resolution NWP.

## Acknowledgements

The authors wish to thank the French National Institute of Geographic and Forest Information for providing ZTD observations in near-real time, and the continued efforts of the E-GVAP and its collaborators. E. Pottiaux also wishes to thank the Solar-Terrestrial Centre of Excellence (STCE) for its support to sustain ROB's contribution to E-GVAP and to this study.

## References

- Andersson E, Fisher M, Munro R, McNally AP. 2000. Diagnosis of background errors for radiances and other observable quantities in a variational data assimilation scheme, and the explanation of a case of poor convergence. *Q. J. R. Meteorol. Soc.* **126**: 1455–1472.
- Bennett GV, Jupp A. 2012. Operational assimilation of GPS zenith total delay observation into the Met Office numerical weather prediction models. *Mon. Weather Rev.* **140**: 2706–2719.
- Bevis M, Businger S, Herring TA, Rocken C, Anthes RA, Ware RH. 1992. GPS meteorology: Remote sensing of atmospheric water vapor using the global positioning system. *J. Geophys. Res.* **97**: 15787–15820. <https://doi.org/10.1029/92JD01517>.
- Boehm J, Niell AE, Tregoning P, Schuh H. 2006a. Global Mapping Function (GMF): A new empirical mapping function based on numerical weather model data. *Geophys. Res. Lett.* **33**: L07304. <https://doi.org/10.1029/2005GL025546>.
- Boehm J, Werl B, Schuh H. 2006b. Troposphere mapping functions for GPS and very long baseline interferometry from European Centre for Medium-Range Weather Forecasts operational analysis data. *J. Geophys. Res.* **111**: B02406. <https://doi.org/10.1029/2005JB003629>.
- Boehm J, Kouba J, Schuh H. 2008. Forecast Vienna mapping functions 1 for real-time analysis of space geodetic observations. *J. Geod.* **83**: 397–401. <https://doi.org/10.1007/s00190-008-0216-y>.
- Bormann N, Bauer P. 2010. Estimates of spatial and interchannel observation-error characteristics for current sounder radiances for numerical weather prediction. I: Methods and application to ATOVS data. *Q. J. R. Meteorol. Soc.* **136**: 1036–1050.
- Bormann N, Saarinen S, Kelly G, Thépaut J-N. 2003. The spatial structure of observation errors in atmospheric motion vectors from geostationary satellite data. *Mon. Weather Rev.* **131**: 706–718.

- Bormann N, Collard A, Bauer P. 2010. Estimates of spatial and interchannel observation-error characteristics for current sounder radiances for numerical weather prediction. II: Application to AIRS and IASI data. *Q. J. R. Meteorol. Soc.* **136**: 1051–1063.
- Bormann N, Geer AJ, Bauer P. 2011. Estimates of observation-error characteristics in clear and cloudy regions for microwave imager radiances from numerical weather prediction. *Q. J. R. Meteorol. Soc.* **137**: 2014–2023.
- Bruyinx C, Habrich H, Söhne W, Kenyeres A, Stangl G, Völksen C. 2012. Enhancement of the EUREF permanent network services and products. In *Geodesy for Planet Earth*, IAG Symposia Series **136**: 27–35. Springer: Berlin. [https://doi.org/10.1007/978-3-642-20338-1\\_4](https://doi.org/10.1007/978-3-642-20338-1_4).
- Dach R, Hugentobler U, Fridez P, Meindl M. 2007. *Bernese GPS Software Version 5.0*. Astronomical Institute, University of Bern: Switzerland.
- Davies T, Cullen MJP, Malcom AJ, Mawson MH, Staniforth A, White AA, Wood N. 2005. A new dynamical core for the Met Office's global and regional modelling of the atmosphere. *Q. J. R. Meteorol. Soc.* **131**: 1759–1782.
- Desroziers G, Berre L, Chapnik B, Poli P. 2005. Diagnosis of observation, background, and analysis error statistics in observation space. *Q. J. R. Meteorol. Soc.* **131**: 3385–3396.
- Desroziers G, Berre L, Chapnik B. 2009. 'Objective validation of a data assimilation system: Diagnosing sub-optimality'. In *Proceedings of Workshop on Diagnostics of Data Assimilation System Performance*. ECMWF: Reading, UK.
- Eresmaa R, Jarvinen H. 2005. Estimation of spatial global positioning system zenith total delay observation error covariance. *Tellus A* **57**: 194–203.
- Garand L, Heilliette S, Buehner W. Interchannel error correlation associated with AIRS radiance observations: Inference and impact in data assimilation. *J. Appl. Meteorol.* **46**: 714–725.
- Guerova G, Jones J, Dousa J, Dick G, de Haan S, Pottiaux E, Bock O, Pacione R, Elgered G, Vedel H, Bender M. 2016. Review of the state of the art and future prospects of the ground-based GNSS meteorology in Europe. *Atmos. Meas. Tech.* **9**: 5385–5406. <https://doi.org/10.5194/amt-9-5385-2016>.
- Herring TA, King RW, McClusky SC. 2009. *GAMIT Reference Manual*, GPS Analysis at MIT - Release 10.3. Department of Earth, Atmospheric, and Planetary Science, MIT: Cambridge, MA.
- Higgins M. 2001. Progress in 3D variational assimilation of total zenith delay at the Met Office. *Phys. Chem. Earth* **26**: 445–449.
- Hollingsworth A, Lönnberg P. 1986. The statistical structure of short-range forecast errors as determined from radiosonde data. Part 1: The wind field. *Tellus A* **38**: 111–136.
- Järvinen H, Andersson E, Bouttier F. 1999. Variational assimilation of time sequences of surface observations with serially correlated errors. *Tellus A* **51**: 469–488.
- Macpherson SR, Deblonde G, Aparicio JM, Casati B. 2008. Impact of NOAA ground-based GPS observations on the Canadian regional analysis and forecast system. *Mon. Weather Rev.* **136**: 2727–2746.
- Niell AE. 1996. Global mapping functions for the atmospheric delay at radio wavelengths. *J. Geophys. Res.* **101**: 3227–3246. <https://doi.org/10.1029/95JB03048>.
- Poli P, Moll P, Rabier F, Desroziers G, Chapnik B, Berre L, Healy SB, Andersson E, El Guelai F-Z. 2007. Forecast impact studies of zenith total delay data from European near-real-time GPS stations in Météo-France 4D-VAR. *J. Geophys. Res.* **112**: D06114. <https://doi.org/10.1029/2006JD007430>.
- Renshaw R, Francis PN. 2011. Variational assimilation of cloud fraction in the operational Met Office Unified Model. *Q. J. R. Meteorol. Soc.* **137**: 1963–1974.
- Rohm W, Yuan Y, Biadeglne B, Zhang K, Le Marshall J. 2014. Ground-based GNSS ZTD/IWV estimation system for numerical weather prediction in challenging weather conditions. *Atmos. Res.* **138**: 414–426.
- Saastamoinen J. 1972. Atmospheric correction for the troposphere and stratosphere in radio ranging of satellites. In *The Use of Artificial Satellites for Geodesy*, Henriksen SW, Mancini A, Chovitz BH (eds.) Geophysical Monograph Series **15**: 247–251. AGU: Washington, DC.
- Stewart LM. 2009. 'Correlated observation errors in data assimilation', PhD thesis. University of Reading: Reading, UK.
- Stewart LM, Dance S, Nichols N, Eyre JR, Cameron J. 2013. Estimating interchannel observation error correlations for IASI radiance data in the Met Office system. *Q. J. R. Meteorol. Soc.* **140**: 1236–1244. <https://doi.org/10.1002/qj.2211>.
- Stoew B, Elgered G. 2005. 'Spatial and temporal correlations of the GPS estimation errors', TOUGH Project report D19. <http://tough.dmi.dk/deliverables/d19-report.pdf>; accessed 4 July 2017.
- Tang Y, Lean H, Bornemann J. 2013. The benefits of the Met Office variable resolution NWP model for forecasting convection. *Meteorol. Appl.* **20**: 417–426.
- Weston P, Bell W, Eyre JR. 2014. Accounting for correlated error in the assimilation of high resolution sounder data. *Q. J. R. Meteorol. Soc.* **140**: 2420–2429. <https://doi.org/10.1002/qj.2306>.
- Wielgosz P, Paziewski J, Baryla R. 2011. On constraining zenith tropospheric delays in processing of local GPS networks with Bernese Software. *Surv. Rev.* **43**: 472–483.